

# PROCEEDINGS OF SPIE

[SPIDigitalLibrary.org/conference-proceedings-of-spie](https://spiedigitallibrary.org/conference-proceedings-of-spie)

## Extended-field synchrotron microtomography for non-destructive analysis of incremental lines in archeological human teeth cementum

Tanner, Christine, Rodgers, Griffin, Schulz, Georg, Osterwalder, Melissa, Mani-Caplazi, Gabriela, et al.

Christine Tanner, Griffin Rodgers, Georg Schulz, Melissa Osterwalder, Gabriela Mani-Caplazi, Gerhard Hotz, Mario Scheel, Timm Weitkamp, Bert Müller, "Extended-field synchrotron microtomography for non-destructive analysis of incremental lines in archeological human teeth cementum," Proc. SPIE 11840, Developments in X-Ray Tomography XIII, 1184019 (7 October 2021); doi: 10.1117/12.2595180

**SPIE.**

Event: SPIE Optical Engineering + Applications, 2021, San Diego, California, United States

# Extended-field synchrotron microtomography for non-destructive analysis of incremental lines in human teeth cementum

Christine Tanner<sup>a,b</sup>, Griffin Rodgers<sup>a,b</sup>, Georg Schulz<sup>a,b,c</sup>, Melissa Osterwalder<sup>a,b</sup>, Gabriela Mani-Caplazi<sup>d</sup>, Gerhard Hotz<sup>d,e</sup>, Mario Scheelf<sup>f</sup>, Timm Weitkamp<sup>f</sup>, and Bert Müller<sup>a,b</sup>

<sup>a</sup>Biomaterials Science Center, Department of Biomedical Engineering, University of Basel, 4123 Allschwil, Switzerland;

<sup>b</sup>Biomaterials Science Center, Department of Clinical Research, University Hospital Basel, 4031 Basel, Switzerland;

<sup>c</sup>Core Facility Micro- and Nanotomography, Department of Biomedical Engineering, University of Basel, 4123 Allschwil, Switzerland;

<sup>d</sup>Integrative Prehistory and Archaeological Science, University of Basel, 4055 Basel, Switzerland;

<sup>e</sup>Natural History Museum of Basel, Anthropological Collection, Basel, 4051 Basel, Switzerland;  
<sup>f</sup>Synchrotron Soleil, 91192 Gif-sur-Yvette, France

## ABSTRACT

Tooth cementum annulation (TCA) is used for determining age-at-death and stress periods based on yearly deposited layers in the root cementum of human teeth. Traditionally, TCA analysis employs optical microscopy, which requires cutting sections of the root and provides only sparse sampling in the third dimension. Ancient teeth are often unique specimens that should not be damaged. In this imaging study, we show that extended-field synchrotron radiation-based microtomography can be used to provide true micrometer resolution and full coverage of the tooth for non-destructively surveying ancient teeth for incremental layers. To rapidly review the root cementum layer of four teeth from an early 19th century cemetery with historical records of life events, we developed a method for automatically enhancing incremental lines on virtual slices and for detecting regions with strong incremental line appearances. Surveying large regions of the root cementum avoids missing high-contrast incremental lines and hence improves TCA analysis as an alternative to irreversible slicing of the unique teeth.

**Keywords:** Synchrotron radiation-based micro computed tomography, mosaic tomography, stitching radiographs, X-ray virtual histology, tooth cementum annulation, dental cementum, enhancement, detection

## 1. INTRODUCTION

Comparable to annual rings in trees and daily layers in otoliths of inner ears,<sup>1</sup> incremental layers are also present in the cementum of human teeth. The layers are most regular in the acellular extrinsic fiber cementum, which is located in the middle third of the tooth root. The contrast of these light and dark bands often correlates well with differences in mineral content, particularly zinc.<sup>2-6</sup> The contribution of variations in collagen orientation detected for goats feed on a controlled changing diet<sup>2</sup> was not confirmed for humans<sup>7</sup> and Beluga whales.<sup>3,6</sup> Latest results for growth bands in Beluga cementum and beaver dentin showed corresponding modulation of carbonated hydroxyapatite (cAp) lattice parameter  $\alpha$ .<sup>6</sup>

As the average width of incremental layers in human teeth is only 3  $\mu\text{m}$ ,<sup>8</sup> we need high-resolution imaging to capture them. Traditionally this is done via physically cutting sections from the tooth and examining local regions with optical microscopy. At high magnification, layers are visible as pairs of dark and light bands, which

---

Further author information: (Send correspondence to C.T.) E-mail: christine.tanner@unibas.ch, Telephone: +41 61 207 54 34, www.bmc.unibas.ch

are called incremental lines. The main drawbacks of this acquisition approach are that teeth are destroyed and only sparse samples can be taken out-of-plane. Incremental lines are used for estimating age-at-death by counting the lines and adding the count to the teeth eruption age. The reported correlations between true and estimated ages are mostly strong,<sup>9</sup> yet reduced accuracies have been observed for an age above 50 years<sup>10</sup> and for teeth with periodontal disease.<sup>11,12</sup> A standardized protocol, sampling several heights and teeth, removing outlier counts and training observers was proposed to help to improve accuracy.<sup>9</sup>

Physically sectioning of the tooth, which is required for optical microscopy, should be avoided for archaeologically valuable teeth. Three-dimensional imaging of the incremental teeth layers by synchrotron microtomography has been proposed to avoid this destruction.<sup>13</sup> Local regions from the tooth cementum were previously imaged via synchrotron microtomography at an isotropic voxel size between 0.33 and 0.62  $\mu\text{m}$ .<sup>13,14</sup> In 2019, Le Cabec et al.<sup>14</sup> investigated the usefulness of synchrotron radiation-based microtomography for estimating the age-at-death of 20 individuals from 20 teeth of an archaeological collection from the 18th to 19th century. They performed two vertically contiguous local scans per tooth. Each took 46 minutes and covered a cylindrical region with a diameter of 1 mm. Two observers independently counted the incremental lines on virtual transverse sections from the region with the better image quality. Overall a moderate correlation of 0.76 was found between real and estimated ages with an average inaccuracy of 16.1 years. The difference decreased to 6.8 years for individuals younger than 50 years.

Finding suitable regions for local tomography is challenging, takes substantial set-up time and missed regions cannot be recovered. As an alternative, we acquired synchrotron microtomograms covering the entire virtual cross-sections of the teeth as well as several height steps with a technique known as extended-field or mosaic tomography. The rationale was to avoid missing regions with good line appearances and to study intra- and interlayer distances. Ultimately this may improve accuracy of age estimation.

The contrast of incremental lines on microscopy images has previously been enhanced by various image post-processing methods. These include contrast stretching, noise reduction, sharpening, and smoothing by Lieberman et al.,<sup>15</sup> band-pass filtering in Fourier space by Czermak et al.,<sup>16</sup> Gabor-cosine band-pass filtering and orthogonal low-pass filtering by Klauenberg et al.,<sup>17</sup> and directional Gaussian filtering by Newham et al.<sup>18</sup> Instead of relying on prior assumptions to enhance certain structures, the 3D images allow us to make the most of the existing 3D structure of the incremental layers to improve incremental line appearance on virtual cross-sections. While we need the high resolution between the layers, we could improve the contrast by integrating along the layers. This approach was applied by Le Cabec et al.<sup>14</sup> by manually rotating the images before projection. Here we additionally account for the curved shape of the layers by automatically straightening them and then automatically determining the optimal direction for integration along the layers.

Our contribution is two-fold. We performed extended-field synchrotron microtomography to capture the whole tooth at sub-micrometer image resolution. Furthermore, we developed a method for automatically improving the appearance of incremental lines, based on integration along the incremental layers for a locally optimal direction.

## 2. MATERIALS AND METHODS

### 2.1 Archeological teeth selection and preparation

Four archaeological teeth from the highly documented 19th-century Basler Spitalfriedhof collection in Switzerland were analyzed using high-resolution microtomography. Age-at-death of the patients was verified<sup>19,20</sup> and the geographical and social origins as well as the family situations for three generations were confirmed genealogically and historically.<sup>20,21</sup> The four teeth came from women with an age-at-death between 30 and 60 years and one or three documented births, see Table 1.

### 2.2 Synchrotron radiation-based X-ray microtomography

We acquired hard X-ray microtomograms of the four ancient teeth at the ANATOMIX beamline, Synchrotron SOLEIL (Gif-sur-Yvette, France).<sup>22</sup> The mean photon energy around 33 keV was selected using 20  $\mu\text{m}$  Au and 100  $\mu\text{m}$  Cu filters and an undulator gap of 5.5 mm. The propagation distance between sample and detector was set to 50 mm. An effective pixel size of 0.65  $\mu\text{m}$  was used. The detector consisted of a 20  $\mu\text{m}$  LuAG scintillator coupled to a Hamamatsu Orca Flash 4.0 V2 scientific CMOS camera (2048  $\times$  2048 pixels, 6.5  $\mu\text{m}$  physical pixel

Table 1. Biographical information related to the imaged teeth.

Tooth	ID	Age	Lifetime	#Births	Tooth Type
T1	Z_1584	36	1829-1865	1	maxillary premolar
T2	Z_1133	30	1816-1846	3	maxillary caninus
T3	Z_823	60	1801-1861	3	maxillary caninus
T4	Z_145	34	1812-1846	1	maxillary premolar

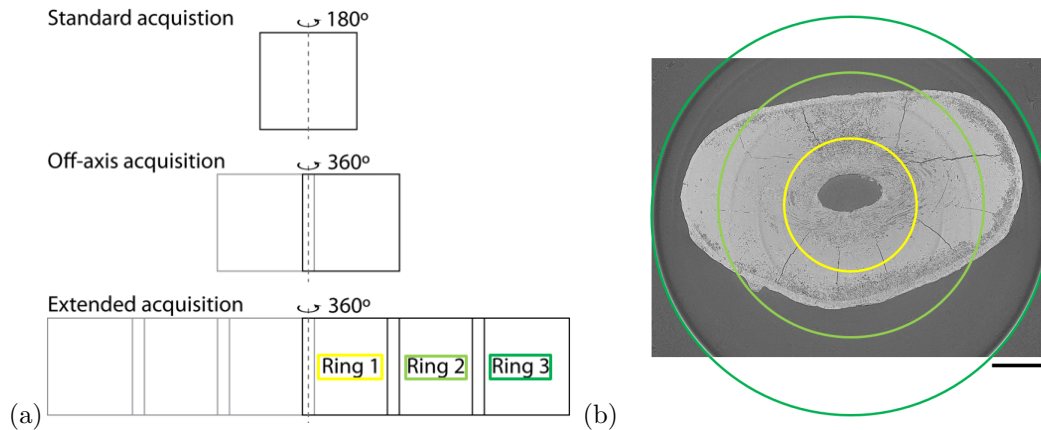


Figure 1. Extended-field acquisition approach. (a) Schematic overview of standard, off-axis and extended acquisition. (b) Example virtual image slice cropped at the top and bottom with illustration of coverage of the three rings. The scale bar is 1 mm.

size) via a  $10\times$  magnifying objective. A complete description of the detector system can be found in Desjardins et al.<sup>23</sup> The exposure time was 100 ms per projection. Each acquisition consisted of 9,000 radiographs over an angular range of  $360^\circ$ .

To capture the whole tooth, we performed extended-field acquisition. In standard acquisitions, the detector is positioned such that the rotation center of the object is projected on a detector column close to the center of the detector field of view. In this case, it is sufficient to take projections over a rotation of  $180^\circ$ , see Fig. 1(a). By putting the rotation center close to the edge of the detector and extending the scan range to  $360^\circ$ , the image extent can almost be doubled. Yet, in our case this still only covers a width of less than 2.66 mm, which corresponds to the area marked by the inner yellow circle in Fig. 1(b). To capture the entire tooth we need to triple the radius of this yellow circle. This was achieved by extended-field acquisition, where we performed three off-center acquisitions and stitched the neighboring radiographs together based on maximizing cross-correlation in the overlapping regions.<sup>24–27</sup> The field of view can be extended in the vertical direction (parallel to the axis of rotation) by stitching reconstructed volumes from multiple height steps.<sup>1,28</sup>

Stitched radiographs were flat- and dark-field corrected. Ring artifacts were removed by low-pass filtering the mean of all projections and subtracting it from the corrected projections.<sup>29,30</sup> Tomographic reconstruction was performed using the open-source toolbox `tomopy` (version 1.4.2)<sup>31</sup> and the `gridrec` algorithm.<sup>32</sup> Note, this reconstruction pipeline is not the standard one used at ANATOMIX. The scan time for a single height steps with three off-center rings, covering a volume of  $7.35\times 7.35\times 1.33\text{ mm}^3$  and consisting of 262 billion voxels ( $11,307\times 11,307\times 2048$  voxels), was 45 minutes. An example slice, cropped at the top and bottom, can be seen in Fig. 1(b).

### 2.3 Enhancement of incremental lines

After image reconstruction and ring correction, incremental lines in the  $0.65\text{ }\mu\text{m}$ -thin-slices often have quite a weak appearance, such that their contrast is insufficient for exhaustive analysis. Yet the incremental lines are actually layers in 3D, as can be seen in the orthogonal slices shown in Fig. 2. The contrast of incremental lines could be improved if we find the right direction to integrate along the curved layers. Hence, we first automatically

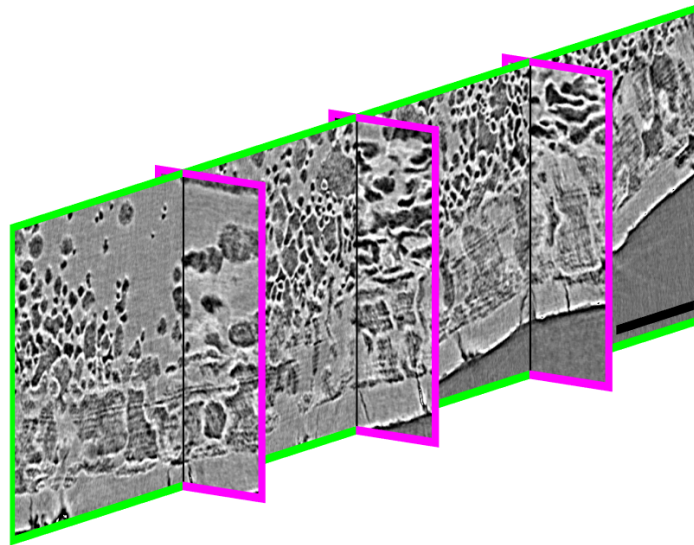


Figure 2. Orthogonal slices showing layer structure. The scale bar in the lower right corner of the image is 100  $\mu\text{m}$ .

straightened the layers to account for their curved shape around the tooth and then searched for an optimal projection direction.

To straighten the cementum, we first semi-automatically segmented the tooth itself. For this we extracted a virtual slab of 55 consecutive transversal slices, corresponding to a thickness of 35.75  $\mu\text{m}$ . We then reduced the slab to a single transversal slice by taking per in-plane pixel the mean of the 55 intensity values along the out-of-plane direction. To reduce noise, we first filtered this mean projection image by a  $15 \times 15$  median filter and then down-sampled it by a factor 15. We automatically segmented the image into background and foreground using Otsu's method, see Fig. 3(a). Next we extracted the tooth region. For teeth with a clear border (teeth T1 and T4), small gaps were filled by morphologically closing the foreground mask using a disk-shaped structure element with radius 10. The largest connected foreground component was extracted to get only the tooth region. For teeth with material attached to the tooth (T2, T3) we first eroded the foreground mask with a disk-shaped structure element of radius 2, 3, or 10 (manually set) to break the attachment. Then the largest connected foreground component was extracted and dilated with the same structure element to get back to the original component size. Finally holes were filled to remove any remaining cracks in the tooth. As we are interested in the cementum, we segmented the outer rim by taking all foreground pixels with a distance of less than 300  $\mu\text{m}$  to the background and selected the largest rim. Then the centerline of the rim was determined. Finally the mask and the centerline was upsampled to the original image resolution. Performing the processing on the downsampled image helped getting a smooth centerline. An example result can be seen in Fig. 3(b).

The next task is to extract subregions of the cementum and straighten these. For this the centerline was sampled clockwise, as indicated by the red line in Fig. 4(a), and the subregion extracted. To straighten the subregion, a cubic spline was fitted to the centerline points and the image was resampled orthogonal to the spline. We used for this the MATLAB implementation by Rolf Harkes.<sup>33</sup> The resampled image was aligned with a predefined coordinate system, such that the tooth border was horizontal and the background region was at the bottom of the image. Finally a standard-sized cementum subregion of size  $750 \times 217 \times 55$  voxels was extracted, see Fig. 4(c). Its intensities were normalized by mapping the range [2nd,98th] percentile to [0,255].

The movie in the supplementary material shows the mean intensity projections when rotating the cementum subregion around the horizontal axis. One can clearly see that the visibility of the incremental lines can greatly be improved for a suitable rotation angle. However, determining this angle manually is time consuming. Therefore we aim for an automatic method to find a rotation angle that improves the incremental line appearances after taking the mean intensity projection. We want to have a good contrast of the incremental lines, which means we want to have a high variation of the intensity values when measuring orthogonal to the incremental lines. Due to the straightening of the cementum and the alignment with the standard coordinate system, the incremental lines

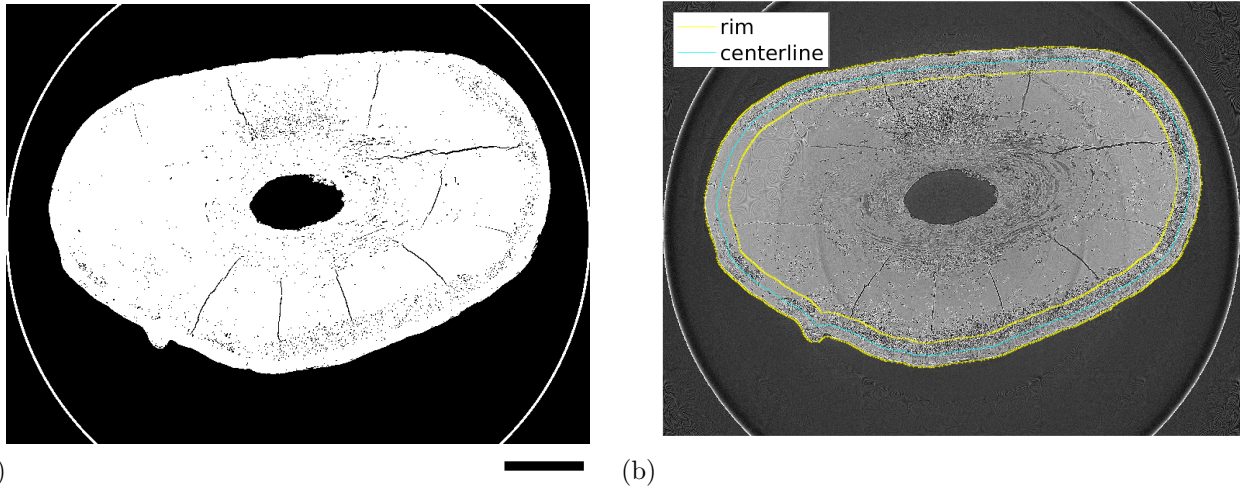


Figure 3. (a) Foreground segmentation after mean intensity projection, median-filtering, downsampling and thresholding. (b) Mean intensity projection image with outer rim mask and centerline contours overlaid. The scale bar is 1 mm.

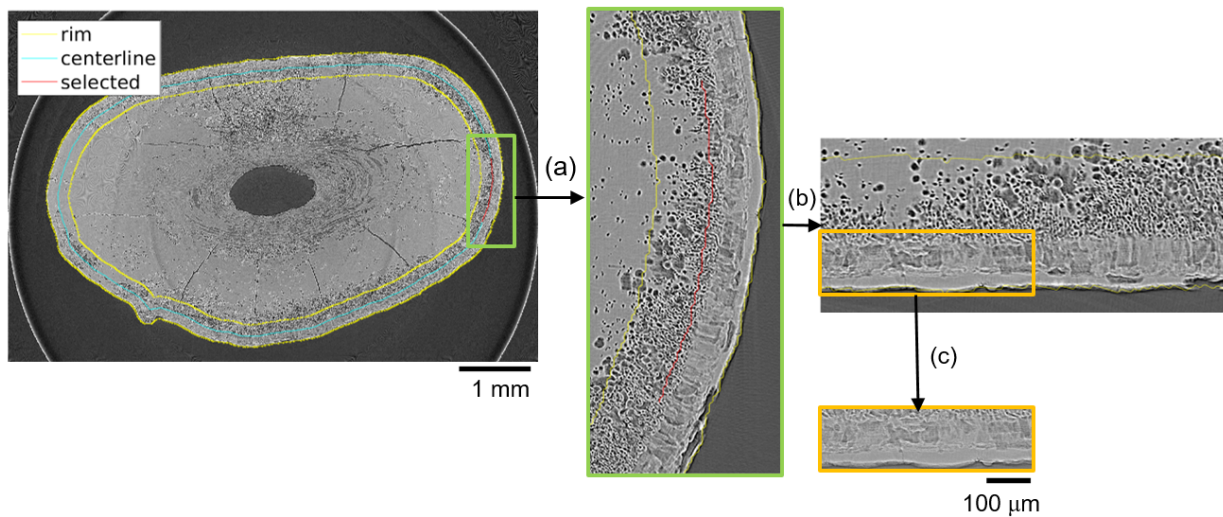


Figure 4. Overview of (a) region sampling, (b) straightening and alignment with predefined coordinate system, and (c) extraction of standard-sized cementum subregion.

are nearly horizontal in the projection images. Therefore we optimized the rotation angle by maximizing the standard deviation along vertical lines in the center of the projection images as shown in Fig. 5(a,b). In Fig. 5(c) one can compare the values of two 1D intensity profiles for both projection images with their standard deviation stated in the legends. As a figure of merit for the visibility of incremental lines as a function of rotation angle, we used the mean of the standard deviations of all 1D intensity profiles, see Fig. 5(d). We evaluated rotation angles from  $-20.1^\circ$  to  $19.9^\circ$  in steps of  $0.5^\circ$ . If this was insufficient, we searched in a 1.5 times larger range, i.e.  $-30.15^\circ$  to  $29.85^\circ$  in steps of  $0.75^\circ$ .

### 3. RESULTS AND DISCUSSION

Example results for the four teeth are shown in Fig. 6. Each of the six panels shows results for the same straightened 3D cementum subregion, namely at the top the center slice, in the middle the projection image for  $0^\circ$ , and at the bottom the projection image for the automatically determined optimal rotation angle. It can be observed that the appearance of the incremental lines was improved by optimizing the rotation angle, i.e. the incremental lines have higher contrast at the bottom than at the top or middle subimage. Quantitatively, the optimization measure increased for these examples in the range of 8.7% to 28.6% over the value for the projection

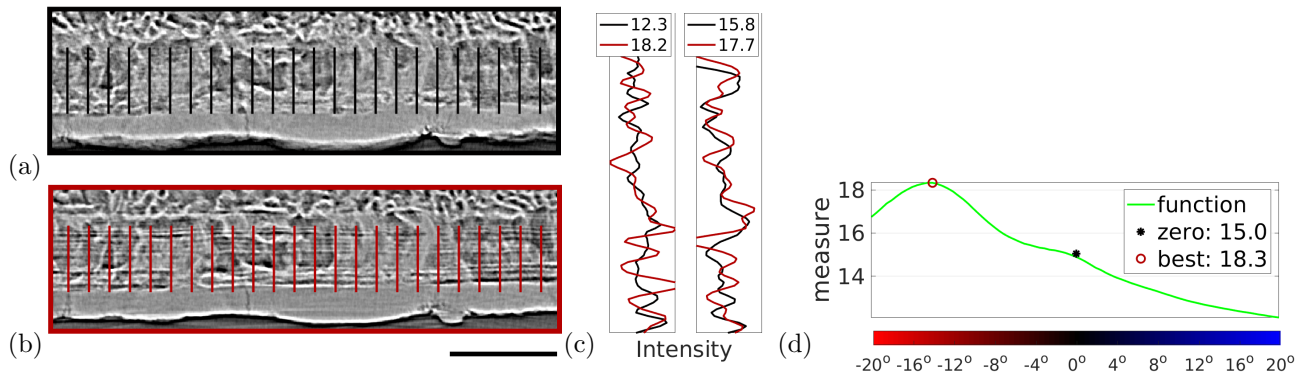


Figure 5. (a,b) Mean intensity projection after rotation by (a)  $0^\circ$  and (b)  $-14.1^\circ$  with location of 1D profiles shown as vertical lines. The scale bar is  $100\ \mu\text{m}$ . (c) Comparison of two 1D intensity profiles from (a) and (b) with standard deviations stated in the captions. (d) Optimization function based on taking the mean of the standard deviations along the vertical 1D intensity profiles per rotation angle. Image intensities were normalized to the range of  $[0,255]$ .

at  $0^\circ$ . Figs. 6(b,d,e) show that the incremental lines after straightening do not have to be perfectly horizontal for this enhancement to work. Interestingly, incremental lines are better visible in darker, lower density, regions than in brighter regions, see Fig. 6(c).

Our method does not improve the incremental lines in all image regions, due to several reasons. In teeth with very homogeneous tissue, like Fig. 6(e,f), incremental lines are often so weak that enhancement still does not make them visible. Sometimes other structures influence the optimization criteria more than the incremental lines, or the 1D profiles in the middle of the subregion might not optimally lie over the incremental lines. However, an enhancement on every subregion is not needed, as the number of incremental lines should be the same for the whole tooth. It is more important to automatically detect a manageable set of subregions, which include high contrast incremental lines. The automatic analysis of the whole cementum for finding regions with high-contrast incremental layers is illustrated in Fig. 7 by the colored disks, which represent the optimization measure (mean of standard deviation of 1D intensity profiles) after optimization. It can be observed that this measure varies relatively smoothly. We investigated selecting per virtual slab the six highest contrast as well as the six most improved subregions based on the optimization measure. Visually inspecting their panels for high contrast examples, like the ones shown in Fig. 6, took less than 5 minutes for 50 panels.

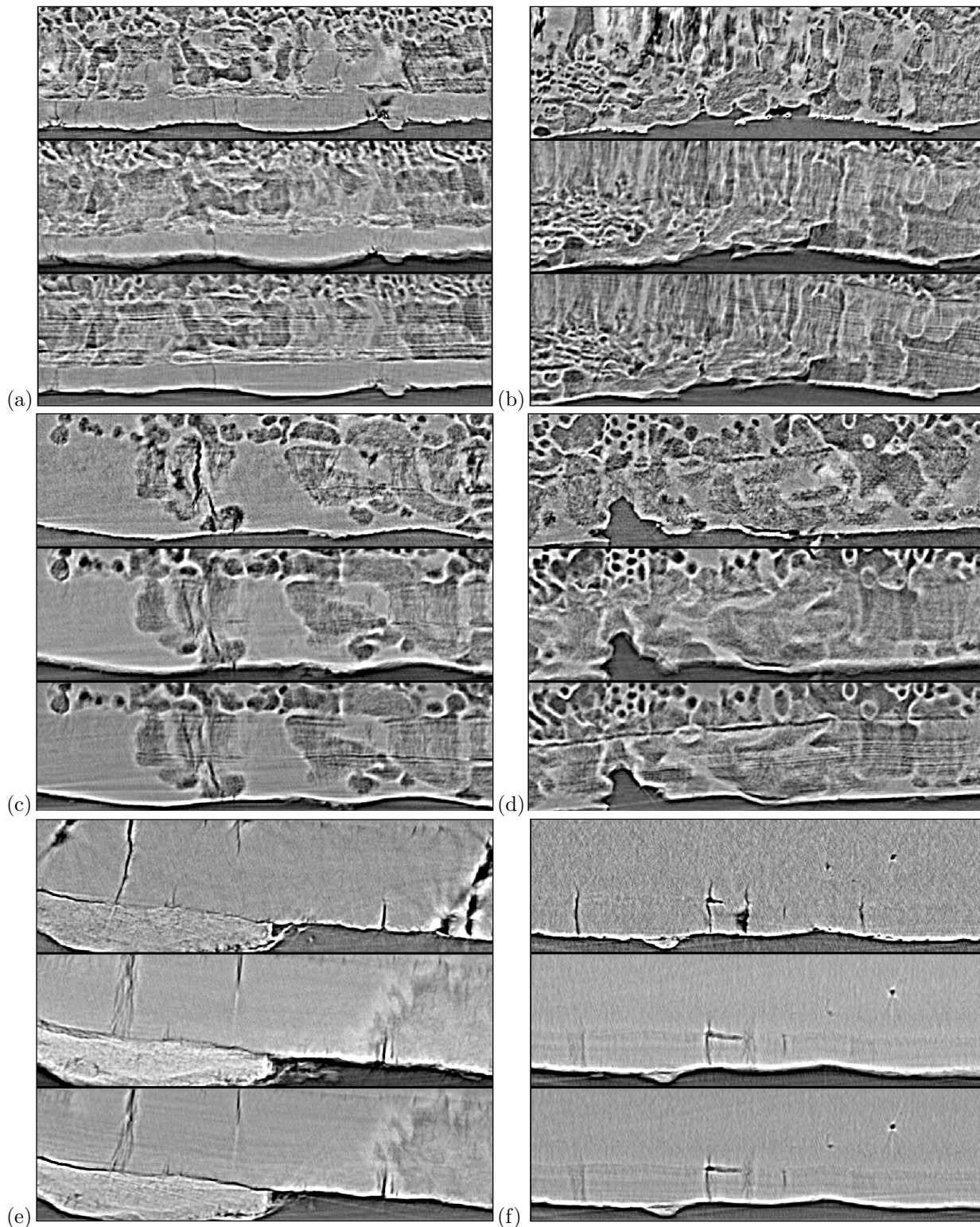


Figure 6. (a-f) Six example results from the four archaeological teeth showing per panel (top) the center slice, (middle) the mean intensity projection at  $0^\circ$ , and (bottom) the mean intensity projection for the optimized rotation angle for the same straightened 3D cementum sub-region. The optimal rotation angle was determined as (a)  $-14.1^\circ$ , tooth T1, (b)  $-8.6^\circ$ , T1, (c)  $9.4^\circ$ , T2, (d)  $18.3^\circ$ , T2, (e)  $-14.1^\circ$ , T3, and (f)  $-8.1^\circ$ , T4. The scale bar is 100  $\mu\text{m}$ .

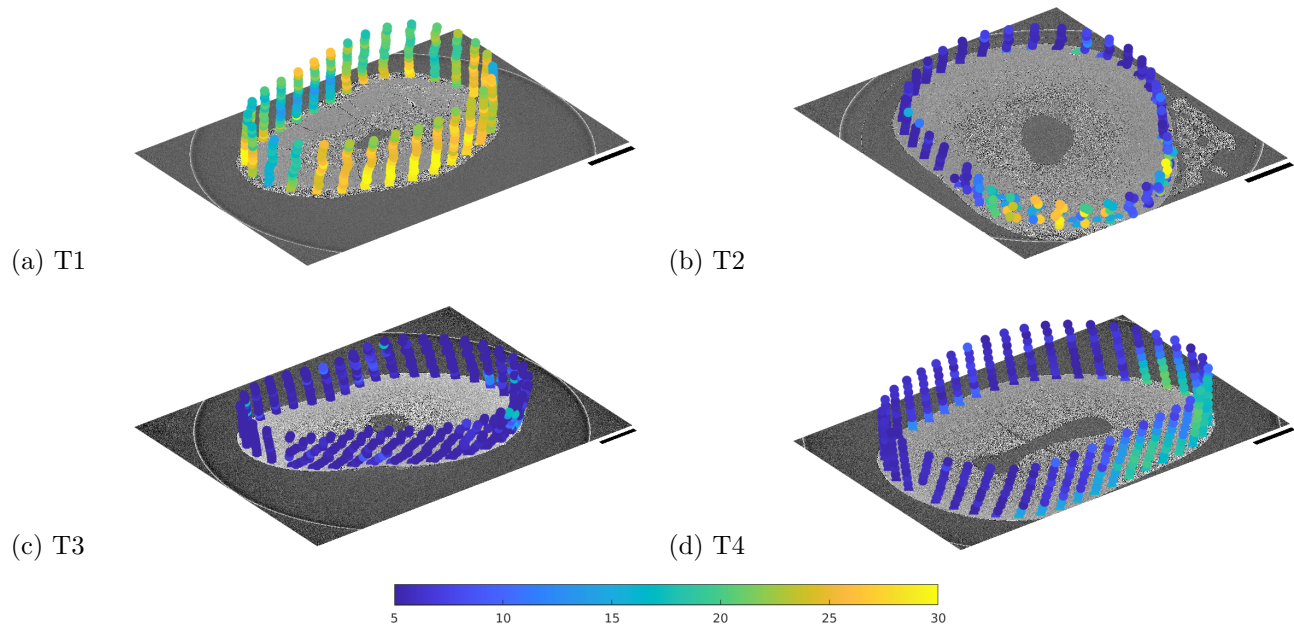


Figure 7. Spatial distribution of optimization measure (mean standard deviation of 1D intensity profiles) shown as colored discs at subregion position for teeth T1 to T4 and various numbers of slabs. The scale bar is 1 mm. Image intensities were normalized from [2nd,98th] percentile to [0,255].

#### 4. CONCLUSION

In conclusion, we acquired synchrotron radiation-based microtomograms that covered the whole tooth on transversal slices thanks to three off-center acquisitions and stitching of radiographs. The acquisition of one height step of 1.3 mm required only 45 minutes, which compares well to the efforts for finding suitable regions for local tomography.

Acquisition of whole cross-sections avoids missing good regions during local tomography. The whole cementum can then automatically be analysed for easier finding regions with high-contrast incremental layers. This was based on maximizing the standard deviation orthogonal to the incremental lines. Additional post-processing, like filtering with the expected spatial frequency to enhance the incremental lines, might benefit this measure.

In this work, we have shown how the appearance of incremental lines can be improved with an automatic method. The key component was to automatically find an optimal rotation angle such that the contrast of incremental lines after mean intensity projection was maximized. This also required extracting cementum regions and straightening them. Projections were performed over a height of 35  $\mu\text{m}$ , since the appearance for smaller or larger heights was generally poorer in initial tests.

The microtomograms could not be compared with corresponding optical microscope images, as the studied teeth were not destroyed and hence no microscope images existed. In future work, we will capture tooth slices with microtomography and then study the correlation between these two image modalities. We did not yet evaluate the accuracy of age estimation as sample numbers are very low and developing an approach to exploit the 3D information for age estimation is beyond the scope of this work.

The improved contrast of the incremental layers will be beneficial for further manual or automatic analysis and the 3D nature of the images will support the study of intra- and inter-layer distances. Overall, extended-field microtomography is a promising acquisition method for non-destructive 3D characterization of the incremental layers.

## 5. ACKNOWLEDGMENTS

We appreciate financial support from the Swiss National Science Foundation (Project No. 185058) and the French National Research Agency (EQUIPEX project *NanoimagesX*, grant no. ANR-11-EQPX-0031). We are grateful for beamtime access at the Synchrotron SOLEIL, ANATOMIX beamline (experiment no. 20200712).

We also thank the Citizen Science Project BBS “Bürgerforschungsprojekt Basel-Spitalfriedhof” for their time-consuming voluntary research regarding the historical sources of the samples.

## REFERENCES

- [1] Müller, B., Bernhardt, R., Weitkamp, T., Beckmann, F., Bräuer, R., Schurigt, U., Schrott-Fischer, A., Glueckert, R., Ney, M., Beleites, T., et al., “Morphology of bony tissues and implants uncovered by high-resolution tomographic imaging,” *International Journal of Materials Research* **98**(7), 613–621 (2007).
- [2] Lieberman, D. E., “Life history variables preserved in dental cementum microstructure,” *Science* **261**(5125), 1162–1164 (1993).
- [3] Stock, S. R., Finney, L., Telsler, A., Maxey, E., Vogt, S., and Okasinski, J., “Cementum structure in Beluga whale teeth,” *Acta Biomaterialia* **48**, 289–299 (2017).
- [4] Naji, S., Rendu, W., Gourichon, L., Cai, Z., and Stock, S., “Cementum ultrastructure, a comparative perspective from synchrotron X-ray scanning: fluorescence and diffraction,” in [*Am. J. Phys. Antropol.*], **162**, 296–296 (2017).
- [5] Dean, C., Le Cabec, A., Spiers, K., Zhang, Y., and Garrevoet, J., “Incremental distribution of strontium and zinc in great ape and fossil hominin cementum using synchrotron X-ray fluorescence mapping,” *Journal of the Royal Society Interface* **15**(138), 20170626 (2018).
- [6] Ryan, J., Stulajter, M., Okasinski, J., Cai, Z., Gonzalez, G., and Stock, S., “Carbonated apatite lattice parameter variation across incremental growth lines in teeth,” *Materialia* **14**, 100935 (2020).
- [7] Cool, S., Forwood, M., Campbell, P., and Bennett, M., “Comparisons between bone and cementum compositions and the possible basis for their layered appearances,” *Bone* **30**(2), 386–392 (2002).
- [8] Mani-Caplazi, G., Hotz, G., Wittwer-Backofen, U., and Vach, W., “Measuring incremental line width and appearance in the tooth cementum of recent and archaeological human teeth to identify irregularities: First insights using a standardized protocol,” *International Journal of Paleopathology* **27**, 24–37 (2019).
- [9] Naji, S., Colard, T., Blondiaux, J., Bertrand, B., d’Incau, E., and Bocquet-Appel, J.-P., “Cementochronology, to cut or not to cut?,” *International Journal of Paleopathology* **15**, 113–119 (2016).
- [10] Bertrand, B., Cunha, E., Bécart, A., Gosset, D., and Hédouin, V., “Age at death estimation by cementochronology: Too precise to be true or too precise to be accurate?,” *American Journal of Physical Anthropology* **169**(3), 464–481 (2019).
- [11] Kagerer, P. and Grupe, G., “Age-at-death diagnosis and determination of life-history parameters by incremental lines in human dental cementum as an identification aid,” *Forensic Science International* **118**(1), 75–82 (2001).
- [12] Dias, P., Beaini, T., and Melani, R., “Age estimation from dental cementum incremental lines and periodontal disease,” *J Forensic Odontostomatol* **28**(1), 13–21 (2010).
- [13] Mani-Caplazi, G., Schulz, G., Deyhle, H., Hotz, G., Vach, W., Wittwer-Backofen, U., and Müller, B., “Imaging of the human tooth cementum ultrastructure of archeological teeth, using hard X-ray microtomography to determine age-at-death and stress periods,” in [*Developments in X-Ray Tomography XI*], *Proceedings SPIE* **10391**, 103911C, International Society for Optics and Photonics (2017).
- [14] Le Cabec, A., Tang, N. K., Ruano Rubio, V., and Hillson, S., “Nondestructive adult age at death estimation: visualizing cementum annulations in a known age historical human assemblage using synchrotron X-ray microtomography,” *American Journal of Physical Anthropology* **168**(1), 25–44 (2019).
- [15] Lieberman, D. E., Deacon, T. W., and Meadow, R. H., “Computer image enhancement and analysis of cementum increments as applied to teeth of *Gazella gazella*,” *Journal of Archaeological Science* **17**(5), 519–533 (1990).
- [16] Czermak, A., Czermak, A., Ernst, H., and Grupe, G., “A new method for the automated age-at-death evaluation by tooth-cementum annulation (TCA),” *Anthropologischer Anzeiger* , 25–40 (2006).

- [17] Klauenberg, K. and Lagona, F., “Hidden Markov random field models for TCA image analysis,” *Computational Statistics & Data Analysis* **52**(2), 855–868 (2007).
- [18] Newham, E., Gill, P. G., Brown, K. R., Gostling, N. J., Corfe, I. J., and Schneider, P., “A robust, semi-automated approach for counting cementum increments imaged with X-ray computed tomography,” *bioRxiv* (2021). preprint on <https://www.biorxiv.org/content/early/2021/03/25/2021.03.25.436951>.
- [19] Hotz, G., Zulauf-Semmler, M., Fiebig-Ebnetter, V., Schumacher, B., Meyer, L., Gysin, D., Gamma, M., Haas, O., Blatter, S., Blatter, R., and Gianola, A., “Neue Quellen zur Skelettserie Basel-Spitalfriedhof – Grundlagen interdisziplinärer Zusammenarbeit: Das Bürgerforschungsprojekt Basel-Spitalfriedhof,” *Bull. Soc. Suisse d’Anthrop* **21**, 9–13 (2015).
- [20] Hotz, G. and Steinke, H., “Knochen, Skelette, Krankengeschichten. Spitalfriedhof und Spitalarchiv – zwei sich ergänzenden Quellen,” *Basler Zeitschrift für Geschichte und Altertumskunde* **112**, 105–138 (2012).
- [21] Pavel, M. and Kumpf, M., “Krank und Arm? Die Krankenakten des Bürgerspitals als Spiegel der Zeit. Sozio-ökonomische und epidemiologische Analysen aufgrund von 19.000 Patientendaten (1843-1868) des Bürgerspitals Basel,” *Basl. Z. Gesch. Altertumskd.* **117**, 144–157 (2017).
- [22] Weitkamp, T., Scheel, M., Giorgetta, J. L., Joyet, V., Roux, V. L., Cauchon, G., Moreno, T., Polack, F., Thompson, A., and Samama, J.-P., “The tomography beamline ANATOMIX at Synchrotron SOLEIL,” *J. Phys. Conf. Ser.* **849**, 012037 (2017).
- [23] Desjardins, K., Scheel, M., Giorgetta, J.-L., Weitkamp, T., Meneglier, C., and Carcy, A., “Design of indirect X-ray detectors for tomography on the ANATOMIX beamline,” in [*Proceedings of the 10th International Conference on Mechanical Engineering Design of Synchrotron Radiation Equipment and Instrumentation (MEDSI 2018), Paris, France*], 25–29 (2018).
- [24] Vescovi, R. F. C., Cardoso, M. B., and Miqueles, E. X., “Radiography registration for mosaic tomography,” *Journal of Synchrotron Radiation* **24**(3), 686–694 (2017).
- [25] Vescovi, R., Du, M., de Andrade, V., Scullin, W., Gürsoy, D., and Jacobsen, C., “Tomosaic: efficient acquisition and reconstruction of teravoxel tomography data using limited-size synchrotron X-ray beams,” *Journal of Synchrotron Radiation* **25**(5), 1478–1489 (2018).
- [26] Du, M., Vescovi, R., Fezzaa, K., Jacobsen, C., and Gürsoy, D., “X-ray tomography of extended objects: a comparison of data acquisition approaches,” *J. Opt. Soc. Am. A* **35**(11), 1871–1879 (2018).
- [27] Miettinen, A., Oikonomidis, I. V., Bonnin, A., and Stampanoni, M., “NRStitcher: non-rigid stitching of terapixel-scale volumetric images,” *Bioinformatics* **35**(24), 5290–5297 (2019).
- [28] Müller, B., Deyhle, H., Lang, S., Schulz, G., Bormann, T., Fierz, F. C., and Hieber, S. E., “Three-dimensional registration of tomography data for quantification in biomaterials science,” *International Journal of Materials Research* **103**(2), 242–249 (2012).
- [29] Boin, M. and Haibel, A., “Compensation of ring artefacts in synchrotron tomographic images,” *Opt. Express* **14**(25), 12071–12075 (2006).
- [30] Mirone, A., Brun, E., Gouillart, E., Tafforeau, P., and Kieffer, J., “The PyHST2 hybrid distributed code for high speed tomographic reconstruction with iterative reconstruction and a priori knowledge capabilities,” *Nucl. Instrum. Methods Phys. Res., B* **324**, 41–48 (2014). 1st International Conference on Tomography of Materials and Structures.
- [31] Gürsoy, D., De Carlo, F., Xiao, X., and Jacobsen, C., “Tomopy: a framework for the analysis of synchrotron tomographic data,” *Journal of Synchrotron Radiation* **21**(5), 1188–1193 (2014).
- [32] Marone, F. and Stampanoni, M., “Regridding reconstruction algorithm for real-time tomographic imaging,” *Journal of Synchrotron Radiation* **19**(6), 1029–1037 (2012).
- [33] Harkes, R., “Straighten an image in Matlab,” (Feb. 2021). <https://ch.mathworks.com/matlabcentral/fileexchange/72266-straighten>.